NINETEENTH EUROPEAN ROTORCRAFT FORUM

Paper C13

INFLUENCE OF INBOARD SHEDDED ROTOR BLADE WAKE TO THE ROTOR FLOW FIELD

by

L. ZERLE, S.WAGNER
UNIVERSITÄT STUTTGART
GERMANY

SEPTEMBER 14-16, 1993
CERNOBBIO (Como)
ITALY

ASSOCIAZIONE INDUSTRIE AEROSPAZIALI
ASSOCIAZIONE ITALIANA DI AERONAUTICA ED ASTRONAUTICA

INFLUENCE OF INBOARD SHEDDED ROTOR BLADE WAKE TO THE ROTOR FLOW FIELD

L. ZERLE and S. WAGNER
Institut für Aerodynamik und Gasdynamik
Universität Stuttgart
Pfaffenwaldring 21, D–7000 Stuttgart 80
Federal Republic of Germany

ABSTRACT

Rotor flow field calculation using the Free Wake Vortex Lattice method allows the isolated investigation of distinct singularities in this flow field. Measurements from a wind tunnel or testbed run always represent the complete flow. The effect of 'inboard wake', produced at the inner radial part of blade's trailing edge, was investigated by means of the CFD–code capability of influence subdivision. In comparison with measurements rotor inflow evaluations produce very similar result diagrams as far as the full wake system is taken into consideration. The result patterns are changed significantly if the inboard shedded part of the wake is not included for inflow calculation . In this case the rearward inflow area is much more uniform and more symmetric to the helicopter roll axis. Theoretical considerations about wake production behind lift producing blades (twisted and cyclic pitch controlled) imply that strong, local concentrated inboard wake vorticies must exist. This is confirmed by comparisons with inflow measurement results.

1. Introduction

Flow field prediction in helicopter rotor aerodynamics requires sufficient wake representation. The actual research and development concentrates on Free Wake Vortex Lattice methods, based on linear potential theory. Self induction within the wake causes vortex motion and vortex roll up, especially nearby the rotor disk. Local rotor inflow airspeed is strongly affected by these moving vorticies. Blade vortex interaction (BVI) effects appear. Investigations of rotor inflow were performed with modern LDA measurement equipment [1] and are now used for code validation [2, 3]. Generally, the total flowspeed of the whole configuration, i.e. blade, wake and fuselage influences together, is achieved by a testbed / windtunnel run . In contrast to this, the CFD - panel code allows to assign and isolate the induced velocity components of every singularity in the flow field. Even parts of the wake system can be cut out and evaluated for isolated investigations.
This work is an application and extension of our free wake vortex lattice code as introduced at the European Rotorcraft Forum in 1992, [2]. A lot of background information about this code is given there and will not be repeated. The effects of inboard wake behaviour were investigated, parallel to the code extension to include panelised fuselages . They are reported here.

2. Theoretical Aspects

Lift producing wings in forward flight generate a typical vortex wake system, which must hold the KELVIN–HELMHOLTZ theorem of vorticity conservation within a fluid. A simple example using lifting line theory is given in figure 2.1. It shows the typical 'horseshoe' vortex system. The gradient of the wing–bound vorticity $\Gamma(y)$ (Fig. 2.1a) gives the density and the strength of the free vorticity in the wake, which is shedded downward from the the wing (Fig. 2.1b).
Testcases as described in [1] with twisted blades under cyclic pitch control in forward flight, were calculated by means of our free wake rotor code. The obtained radial doublet strength distribution represents the intensity of the bound vortex along the blade spanwise direction. Figures 2.2a–2.2d give typical distributions at different azimuthal positions (0, 90, 180 and 270 degrees). Due to individual flow situations in

forward flight at each given position, the lines in the diagrams look differently. With respect to the theory described before, the high gradients in the inner radial region of the 0 and 180 degree position indicate a strong inner wake vortex, similar to the strength of the outer tip vortex. The doublet strength at 90 degree inboard position is smoother, but shows a typical blade vortex interaction at 0.65 relative radius. Fig. 2.2d at 270 degree position is the situation of a retreating blade with very low doublet strength in the inner radial area, obviously nearby the point of reverse flow.

A wake system plot of a two bladed rotor in mu = 0.15 forward flight is given in figure 2.3. This rotor performed 1 3/4 revolutions and is in cyclic steady state condition. A typical inboard wake vortex loop is visible in the inner rear area of the actual rotor disk . It is shedded from the inner part of blade's trailing edge, and demonstrates wake roll up activity. As described above, these vorticies are strong and affect the rotor flow field in two important aspects.
1) The induced velocity within this slim loop is high, upward directed and boosts against the general rotor downwash like a small vulcano. In chapter 4 this will be discussed in more detail.
2) Vorticies of this loop are close together and influence each other directly. This results in a self induced motion, like a smoke vortex ring blown into free air. Inboard wake vortex loops tend to move upward against the downwash, and enlarge their effects by approaching to the rotordisk area. Plots of long term wake development in figure 2.4 give a good impression of this kind of movement. The inboard wake of the one bladed rotor demonstrates its upward movement, additionally assisted by the tip vorticies in this special case. This event confirms the necessity of free wake calculation in the rotor code. Inflow velocities proved to be very sensitive to vertical wake positions.

3. Procedure Details

All calculations were done with the free wake vortex lattice code as introduced in [2]. Wake is generated and developed, timestep by timestep without any iteration or relaxation. After each timestep the whole blade and wake systems are stored in a datafile. Detailed evaluations like inflow velocties are performed by a postprocessor at distinct timesteps. For inboard wake investigation the inner four wake and blade vortex filaments were switched off in the post processor only (Fig. 3.1). Mean inflow data as used for comparisons with NASA measurements are produced by averageing of multiple timestep results at the same collocation point position. All calculations were carried out at an isolated rotor without fuselage effects. The coordinate system in figure 3.2 is representative for all following result diagrams. Positiv LAMDA inflow speed (Vertical to the rotor disk and related to rotor tip speed) points upward in quasi z-direction. The collocation point area is a rotor centered disk one cord length above the rotor tip path plane.

4. 2-Bladed Rotor Results

A 2-bladed 2MRTS rotor was used in order to obtain a first impression with a not too complicated wake lattice. Rotation and cyclic pitch control data were the same as used for the 4-bladed rotor tests in [1]. Instead of the full vortex lattice system, figure 4.1a gives the actual rotor position and the boundaries of the wake lattice at the moment of inflow evaluation. These wake boundaries are a good representation of the actual position of the strong tip and inboard vorticies and avoid that the image becomes too complex.
The LAMDA velocity field (complete vortex lattice influence) induced accordingly, is demonstrated in 4.1b , where the induction of both blades at 90 and 270 degree azimuthal position are of good visibility. Strong tip vortex induction causes the jump along the curved line in the front rotor disk section.
Effects of inboard wake activity are demonstrated best by use of the isolated evaluation of the inner four vortex filaments at the collocation points. Diagramm 4.1c shows the main influence of isolated inboard wake in the disk rear position. The main influence is exerted in the area above the vortex loops indicated in figure 4.1a by flag No.1 . The observed upwash peak of lamda = 0.0250 (value 9) is very high and reaches the same size as inductions of the tip vorticies at the outer radial sections of diagram 4.1b (complete induction). We obtain figure 4.1d with a relative symmetric rotor downwash area in the rear disk section if we switch

off the blade inboard shedded wake.
A superposition of fig. 4.1c and 4.1d results in fig. 4.1b with the typical unsymmetry of downwash around the x-axis in the rear disk section ($x/R > 0$). Additionally to that, the inboard vortex parts produced by the forerunning blades superposition to a quasi third vortex line parallel to the x-axis (flag 2 in fig. 4.1a). This enlarges the downwash in the rear, right (starboard) disk section were $y/R > 0$. Downwash level 6 in figure 4.1c and the remarkable shift of level 3 in the rear area of figures 4.1d and 4.1d are typical effects of inboard wake contribution.

5. 4–Bladed Rotor Results / Measurement Comparisons

Calculations with 4–bladed rotors at different advance ratios were performed and compared with LDA measured inflow data [1]. They are plotted in figures 5.1, 5.2, 5.3 for three different advance ratios. As already described in [2] the measurements coincide well with the free wake calculations in tendency, see the diagrams of rotor inflow disk 5.1ab, 5.2ab, 5.3ab .

A discrepancy is observed in the level of the induced inflow speed. That may be caused by the missing fuselage and other effects. Measurement and free wake calculation show the same unsymmetries along the x-axis as described in chapter 4. Due to neglection of the blade inboard wake activity, the downwash reduction in the rear vanishes and the location of maximum downwash shifts to the rear left side at all three investigated advance ratios (Fig. 5.1c, 5.2c, 5.3c).
Line diagrams along discrete azimuthal positions (part d,e,f,g of Fig.5.1, 5.2, 5.3) indicate that in case of disabled inboard wake calculation the tendency of the lamda value remains the same, but the deviation increases at smaller radial positions. Line 'FW noIBW' represents the calculation without inboard wake. At low advance ratio 0.15 the deviation is greater than at 0.23 or 0.30. In this case the upward moving inboard wake loop remains longer within the rotordisk and covers a greater area, which increases its influence.

6. Important Assumptions and Simplifications

1) Linear potential theory is used for the time–stepwise working simulation code. Quasi steady state conditions were assumed within every timestep.
2) For induction evaluation, a vortex core model is used to damp induced velocity within a given radius around the vortex core. That is the single empirical input parameter for the whole code.
3) Rotor blades are modeled with flat doublet panels and constant doublet strength on each panel. A geometrical transition from blade profile to blade root is not included.
4) Reverse flow detection at the retreating blade's inner side is performed. The blade panel doublet strength and the shedded wake doublet strength are set to zero, when reverse flow occurs at that panel.

7. Conclusions

Additionally to tip vortex influences, helicopter flow fields are strongly affected by vorticies which are shedded near the inner radius of the profiled blade part. In spite of a very simple geometrical blade model at the inner location as described above, calculated effects are also observed in measurements. All rotor inflow discontinuities cause pressure and lift oscillations accompanied by vibration and noise generation. It seems that inboard wake effects participate there, too.

References

[1] J.W. Elliott, S.L. Althoff, and R.H. Sailey. *Inflow Measurement Made with a Laser Velocimeter on a Helicopter Model in Forward Flight.* Technical Memorandum TM 100541–100543, NASA Langley Research Center, Hampton, Virgina 23665–5225, 1988.

[2] L. Zerle and S. Wagner. *Development and Validation of a Vortex Lattice Method to Calculate the Flowfield of a Helicopter Rotor Including Free Wake Development.* In *Proceedings of the 18. European Rotorcraft Forum*, Avignon, France, September 1992. Paper No. 72.

[3] L. Zerle, und S. Wagner. *Rotor - Rumpf Interferenzuntersuchung durch Kopplung eines Wirbelgitterverfahrens für den freien Nachlauf mit einem einfachen Verdrängungskörpermodell.* In *Tagungsband des 8. DGLR–Fach–Symposiums*, Köln–Porz, November 1992.

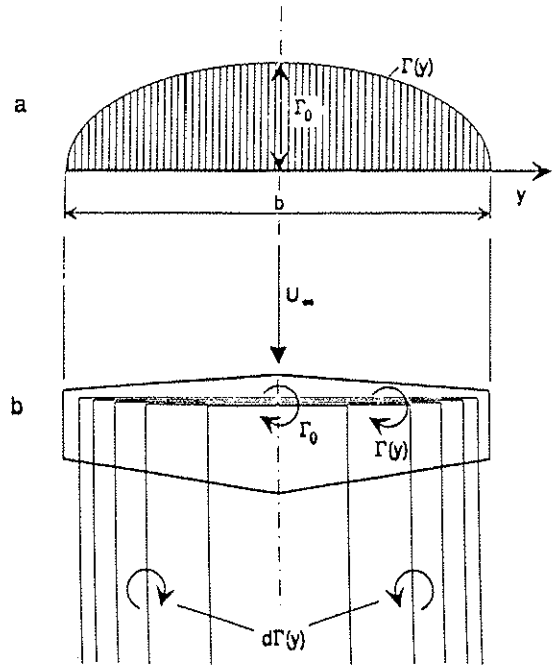

Fig. 2.1

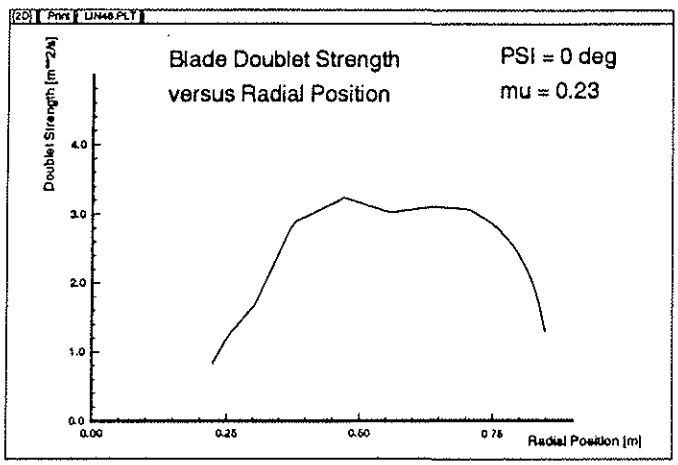

Fig. 2.2a

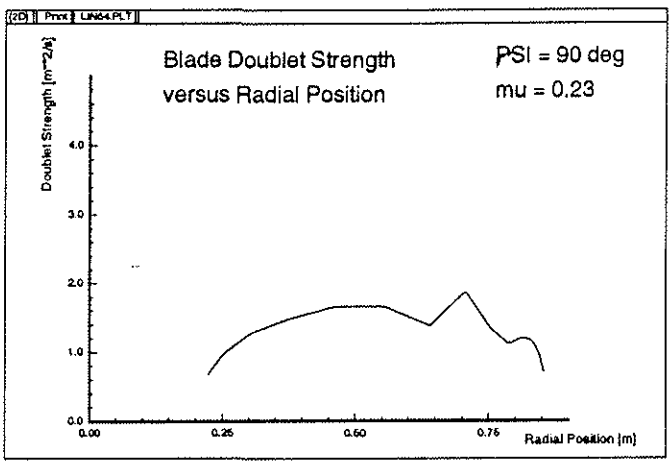

Fig.2.2b

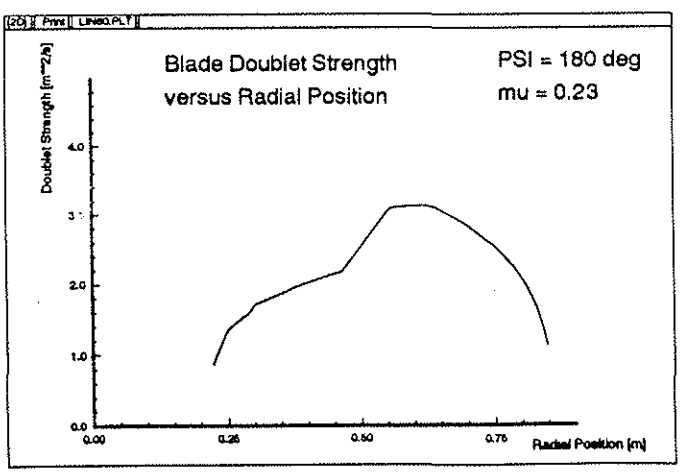

Fig. 2.2c

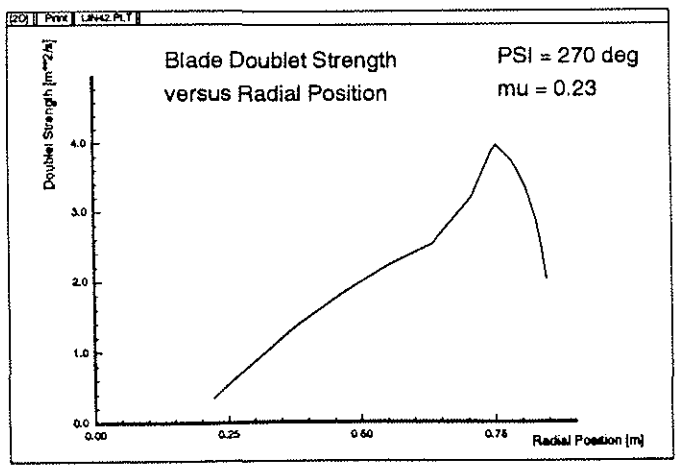

Fig. 2.2d

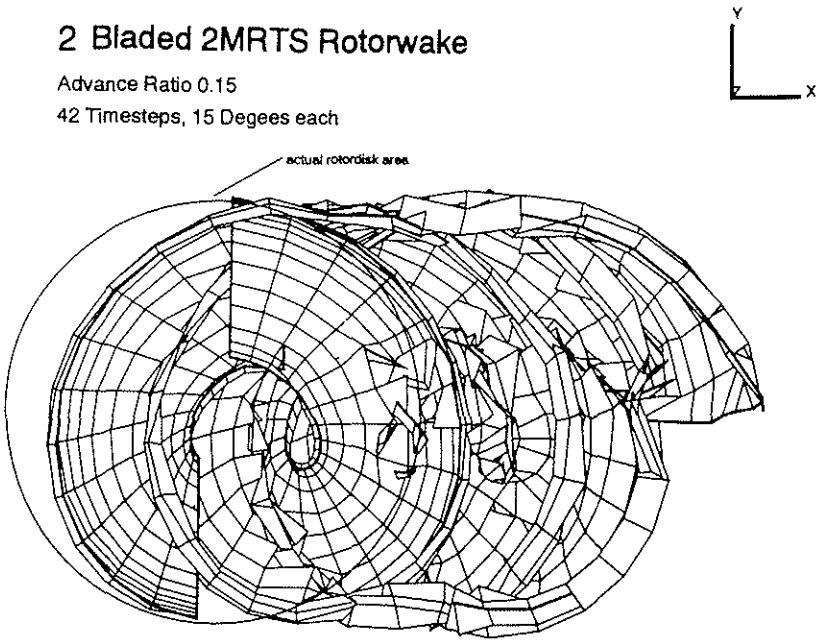

Fig. 2.3

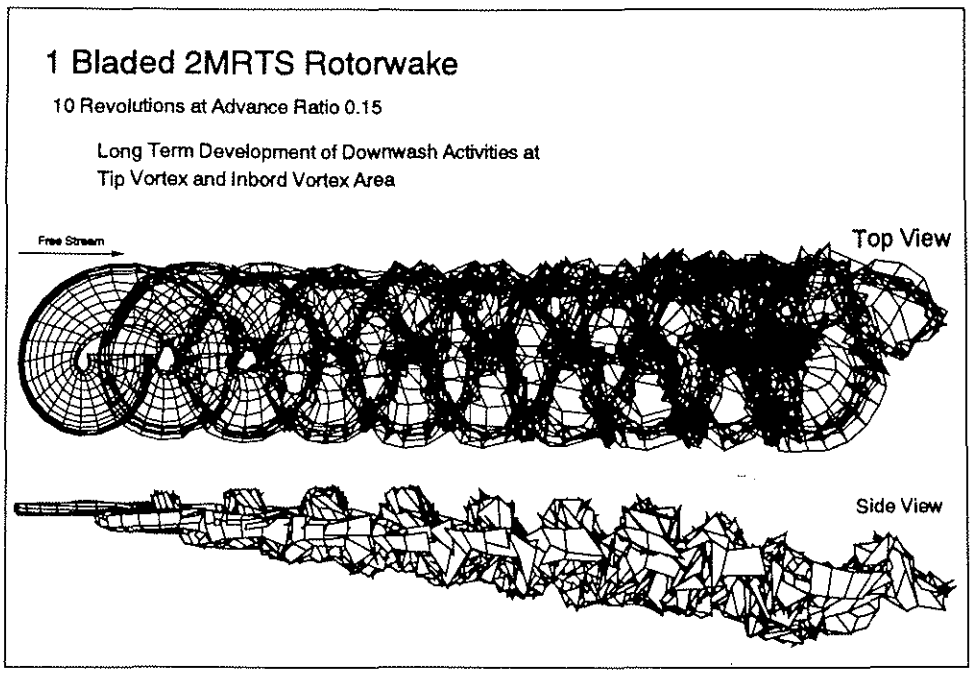

Fig. 2.4

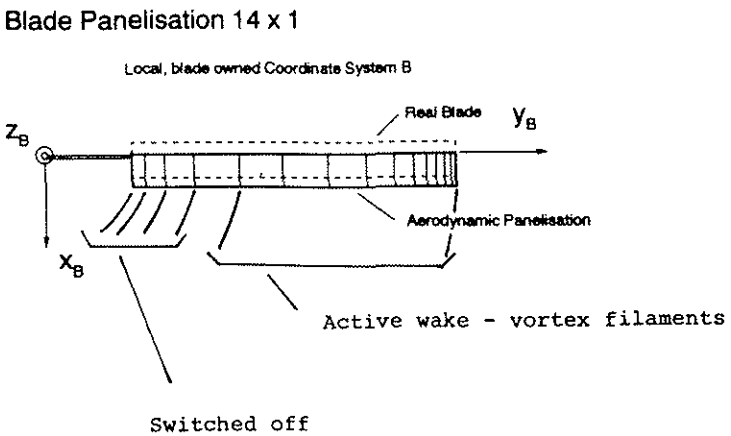

Fig. 3.1

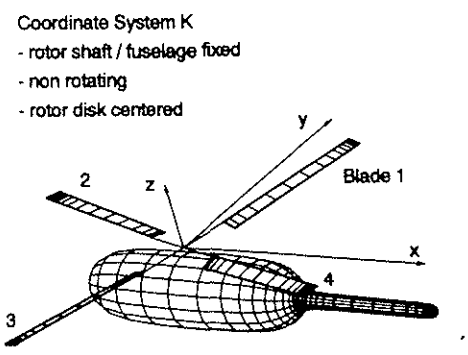

Fig 3.2

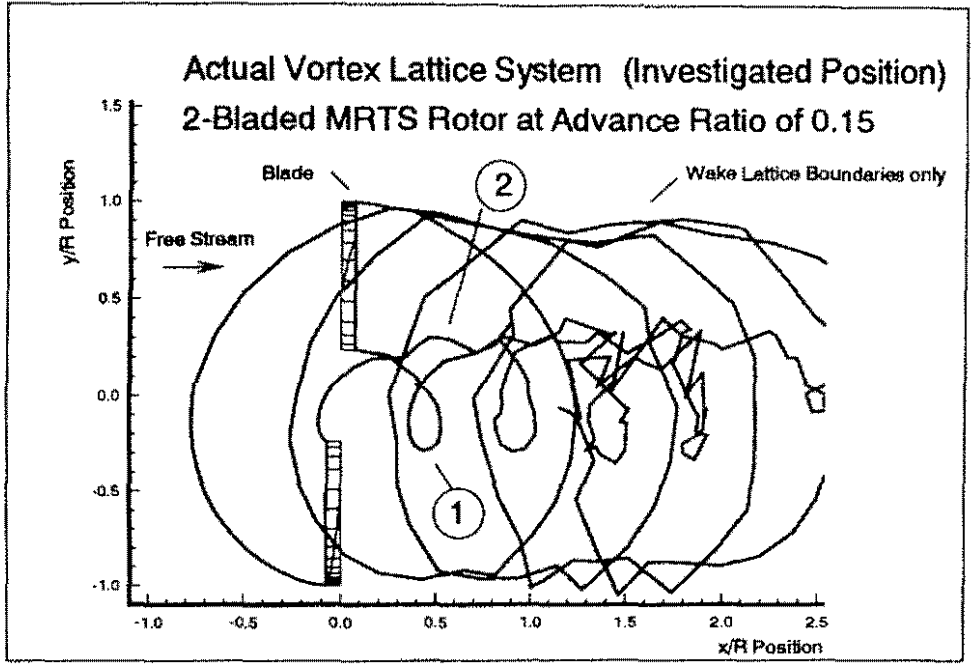

Fig. 4.1a

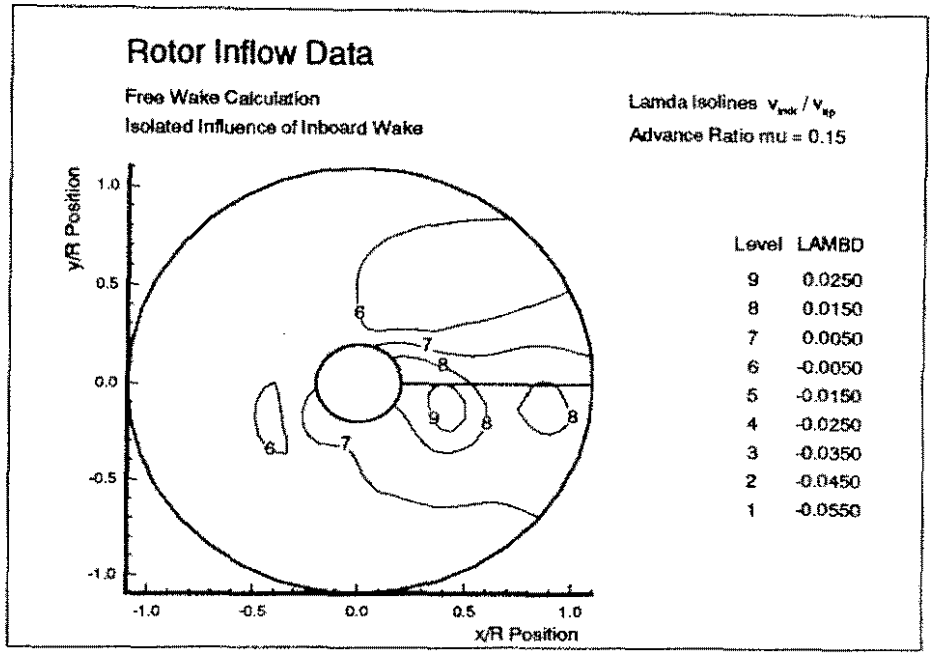

Fig 4.1c

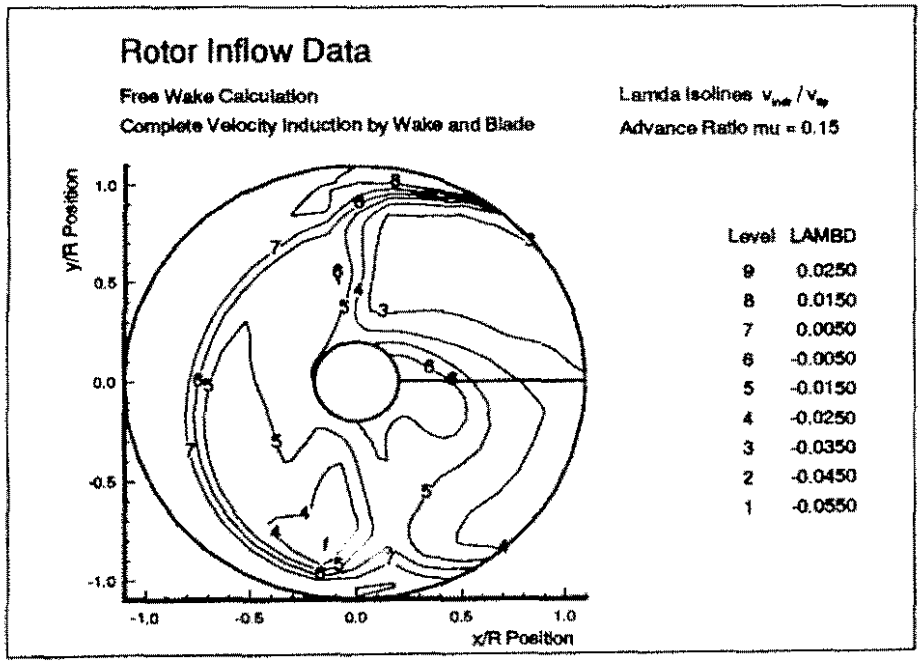

Fig. 4.1b

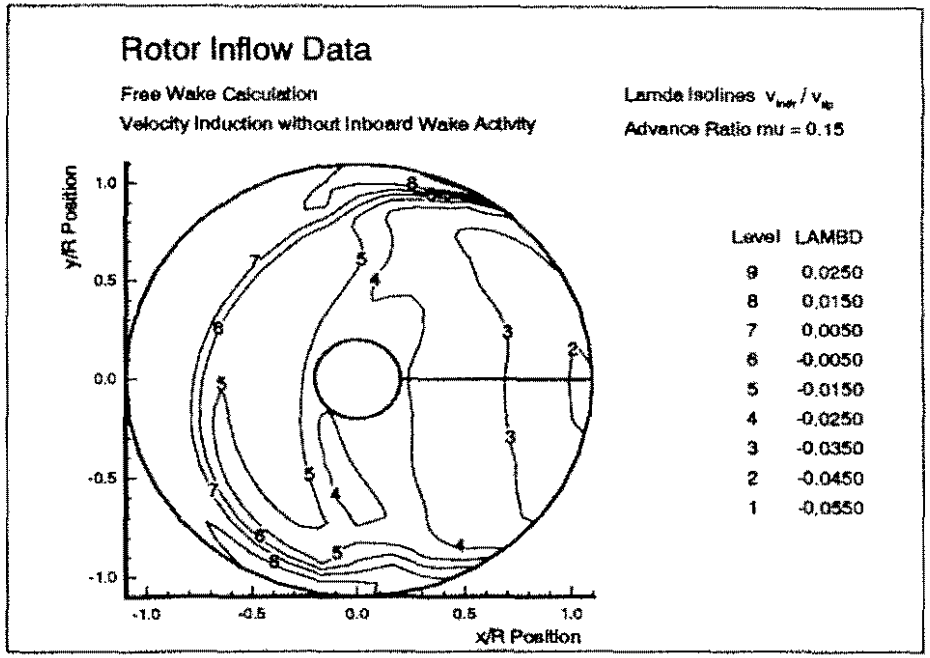

Fig. 4.1d

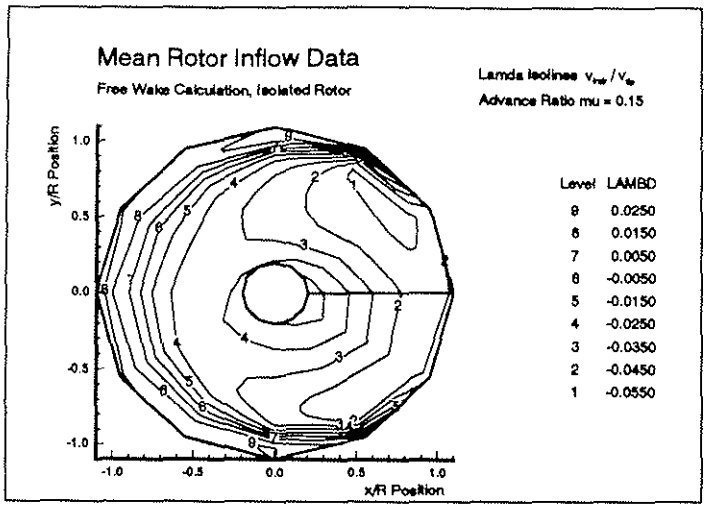

a

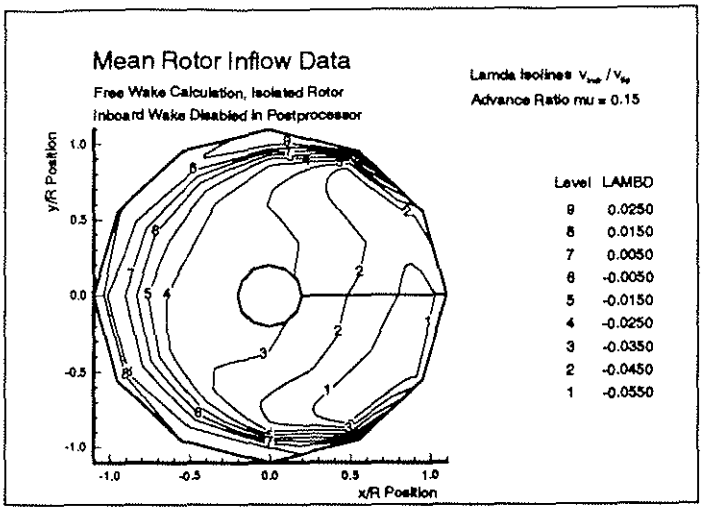

c

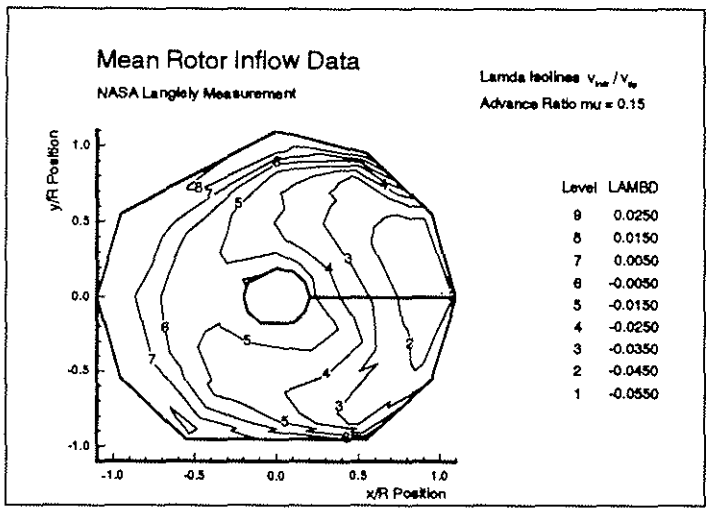

b

Fig. 5.1

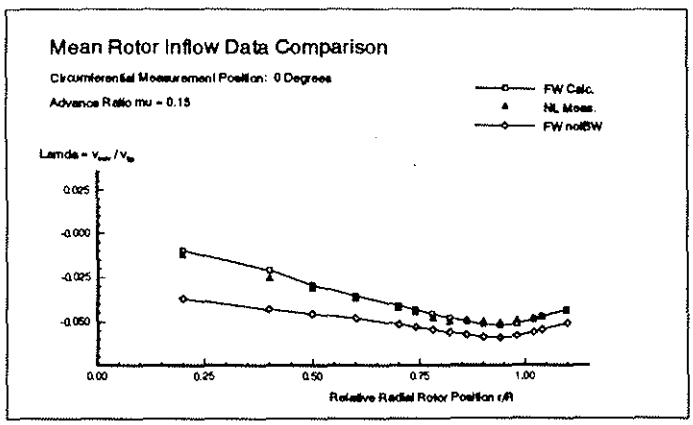

d

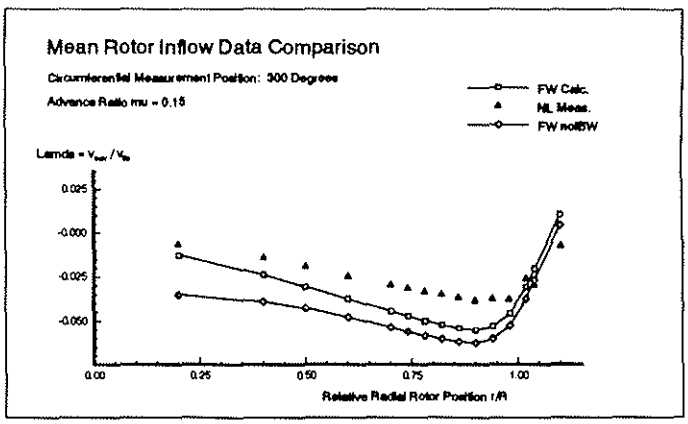

e

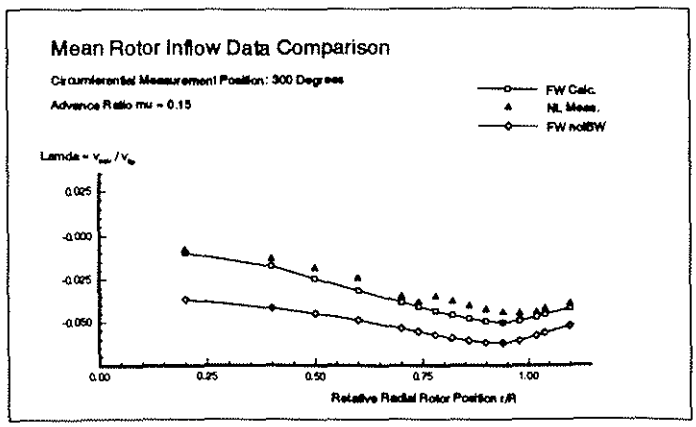

f

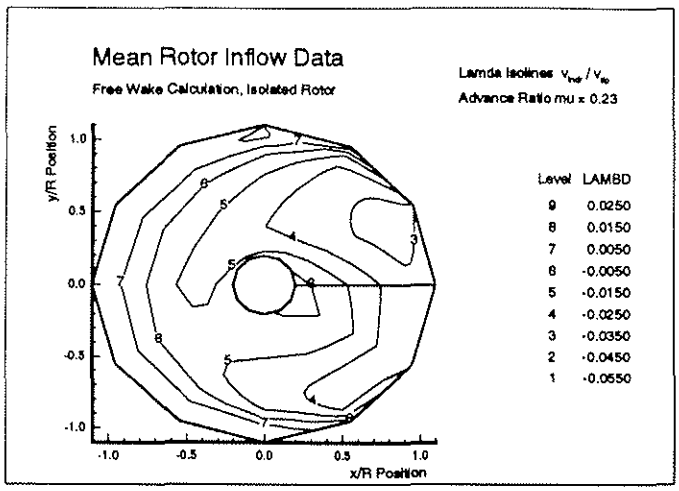

a

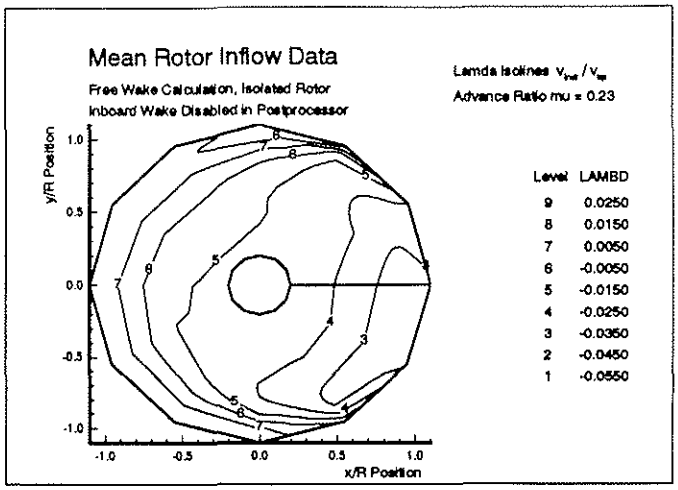

c

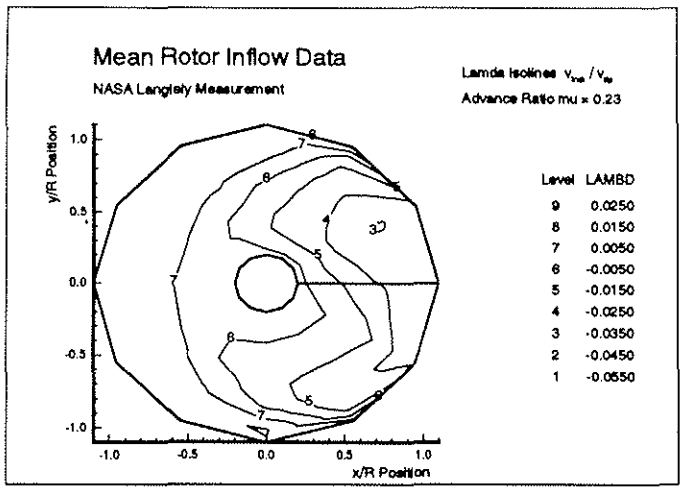

b

Fig. 5.2

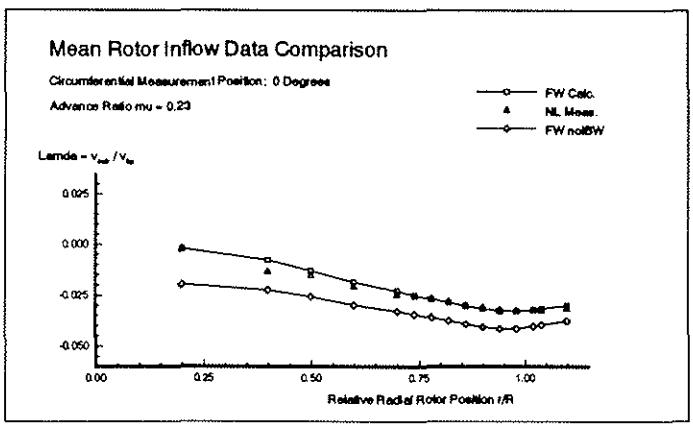

d

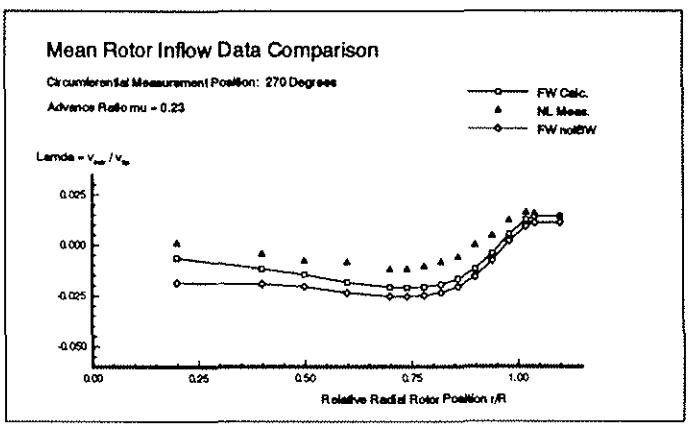

e

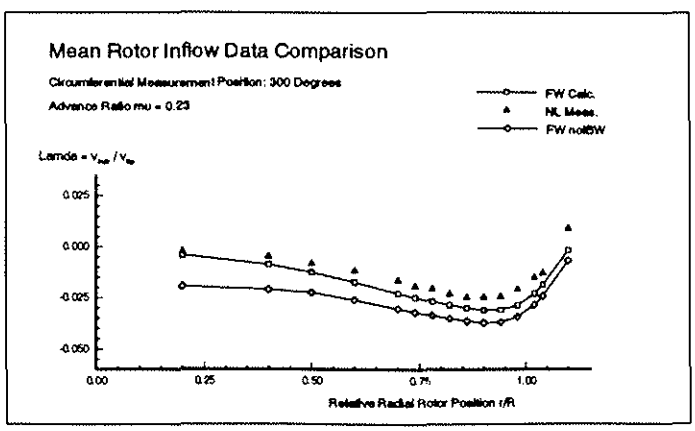

f

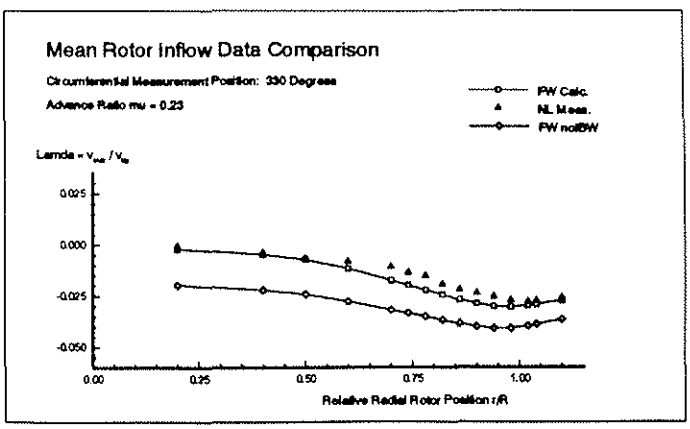

g

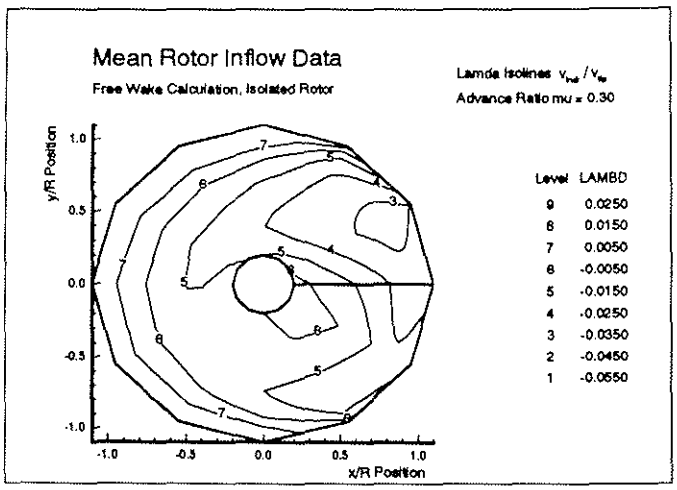

a

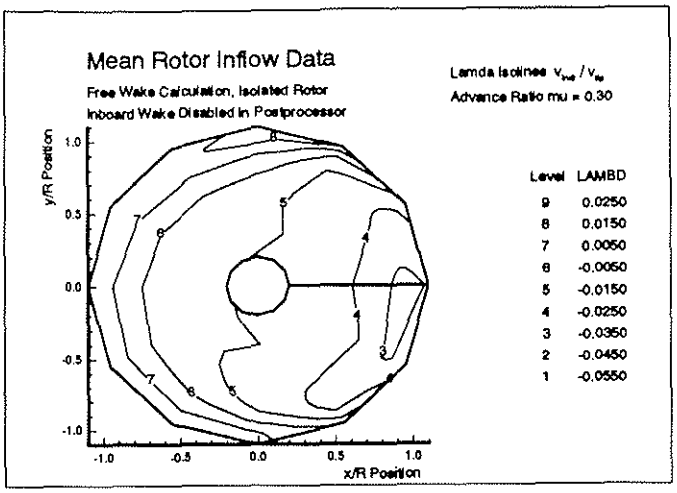

c

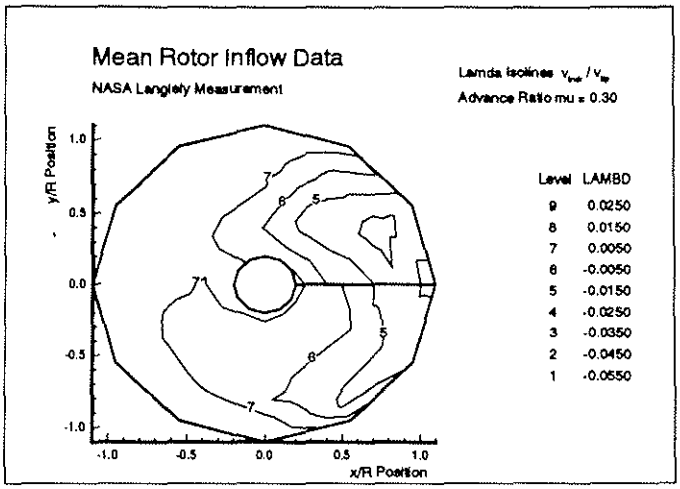

b

Fig. 5.3

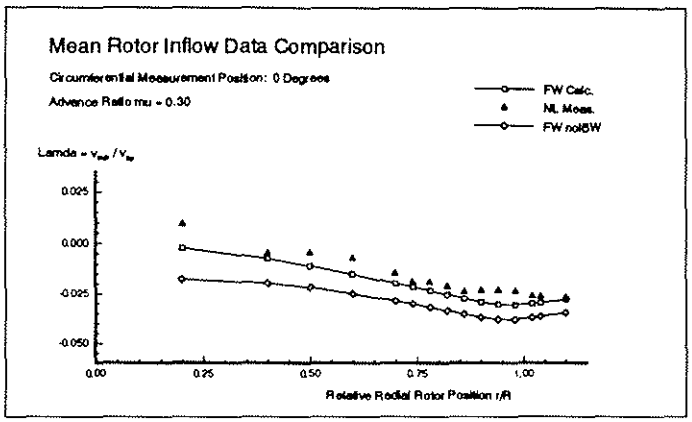

d

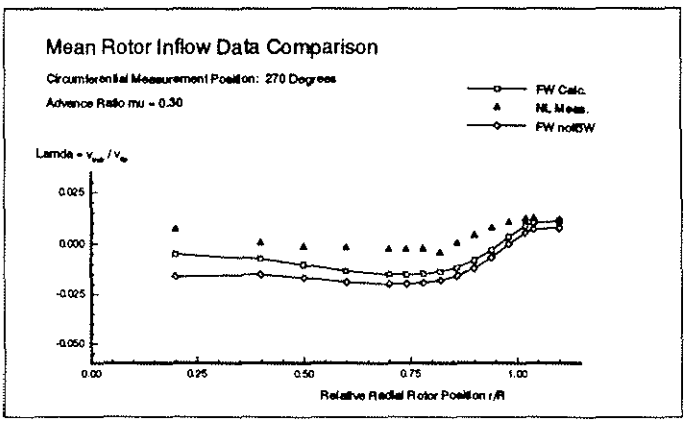

e

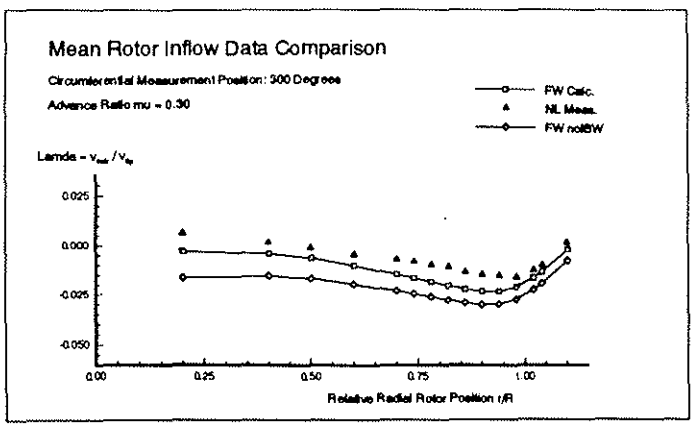

f

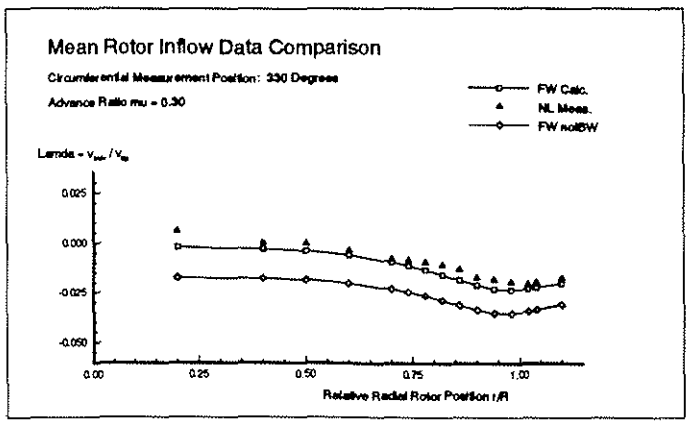

g